Effect of Objective Function Formulation on Static and Operating Parameters of a Switched Reluctance Motor After Optimization of Magnetic Circuit Shape

Krzysztof WROBEL, Krzysztof TOMCZEWSKI
Institute of Drive Systems and Robotics
Opole University of Technology, Opole, 45-758, ul. Proszkowska 76,
k.wrobel@po.opole.pl

***Abstract*—The article presents a comparison of two optimization methods aimed at the linearization of electromagnetic torque on rotor position angle in a two-phase switched reluctance motor (SRM). To optimize the shape of the SRM magnetic circuit, two objective functions were used, dependent on average, minimum and maximum values, and standard deviation electromagnetic torque. For computations, Matlab software was used along with the GAOT library. Parallel computations were carried out using the HTCondor environment. Optimization results were assessed by comparing the electromagnetic torque waveforms of the obtained SRM designs at different points of the drive operation. As a result of the research, additional criteria for assessing the quality of the drive in terms of pulsation of the electromagnetic torque are proposed.**

***Index Terms*—cost function, magnetic circuits, optimization, variable speed drives, torque, switched reluctance motor.**

I. Introduction

Due to the silent-pole design of typical SRMs and pulse supply, such drives are characterized by a high level of electromagnetic torque ripple, and consequently by high level of vibrations and noise as well [1, 2]. The amplitude of the electromagnetic torque oscillations is influenced by both, motor design parameters and the supply method [3-6]. Torque ripples are one of the basic problems when designing motors and drives of this type. Reducing them is one of the main tasks involved in designing this kind of motor. Achievement of favourable static characteristics [7-9] does not ensure acquisition of favourable parameters during drive operation.

Among motor design parameters with the most significant impact on its operation, including the amplitude of torque ripple, is the number of stator poles and rotor teeth. Machines with a large number of poles in the stator and rotor teeth are characterized by the lowest level of torque ripple [10-13]. These are usually low-speed designs.

Another way of shaping the static characteristics of electromagnetic torque or minimizing its pulsation involves motors with a laminated rotor [14-16].

On the other hand, a design characterized by the capacity to obtain maximum rotor speeds, and simultaneously, by the highest level of electromagnetic torque ripple, incorporates a small number of stator poles and rotor teeth, e.g. a phase motor with four stator poles and two rotor teeth. The classic cylindrical rotor design of this type of motor includes regions where the resultant electromagnetic torque is close to zero. In these positions, this type of motor has no starting torque. In order to eliminate this defect in motors with this design, rotor teeth shape asymmetry is introduced [17, 18]. This enables acquisition of positive torque over the whole range of the angle of rotation in which the phase is supplied. Due to this asymmetry, motors of this type are designed to operate in one direction of rotation.

In practice, this asymmetry is more frequently achieved by moving away from the typical cylindrical shape of the rotor teeth by drilling them or by modelling the external surface of the rotor and stator teeth [7, 18-20]. Such a design is applied in the motor optimized in this paper.

II. Optimizing the Shape of Magnetic Circuit

Optimizing the shape of the SRM's magnetic circuit is a multidimensional issue, in which the objective function is nonlinear. Assuming that the only discrete decision variables are the parameters determining motor type, such as the number of rotor teeth and phases, then for a specific-design motor with a fixed number of rotor teeth and stator poles, this question can be formulated as:

$$\max_{\mathbf{w}} \mathbf{z}(\mathbf{w}) \Big|_{\mathbf{w}\in \boldsymbol{W}\subset \mathbf{R}^{n_x}}, \tag{1}$$

where $\mathbf{R}^{n_x}$ is the continuous decision variable space and $\boldsymbol{W}$ is the range of feasible solutions, defined as:

$$\boldsymbol{W} = \{\mathbf{w} : \mathbf{g}(\mathbf{w}) \le 0,\ \mathbf{h}(\mathbf{w}) = 0,\ \mathbf{g} : \mathbf{R}^{n} \to \mathbf{R}^{m'_i}\} \tag{2}$$

where $\mathbf{R}^{n}$ is n-dimensional Euclidean space, and $\mathbf{g} \in \mathbf{R}^{m'_i}$ is inequality restriction vector m'_i. During the optimization of the magnetic circuit of the studied SRM performed within this study, only inequality limitations were applied. The imposed limitations include both ranges of the decision variable and limits of acceptable changes to machine parameters.

Electromagnetic field distribution was calculated with a finite element method (FEM) computer program. For a given value of phase current and angular position of the rotor, the electromagnetic torque was determined with the use of the Maxwell stress tensor. Additionally, electromagnetic flux was calculated for each motor phase. The obtained values were then used to determine the

Digital Object Identifier 10.4316/AECE.2018.03004

objective function, and were also used in the simulation for calculating the waveforms.

When searching for a SRM design characterized by a high average value of electromagnetic torque with low ripple amplitude, the objective function can be formulated as:

$$f = \Pi f_i, \tag{3}$$

where f_i – elementary functions defining the quality of the selected SRM parameters. This approach enables the elimination of time-consuming calculations of weighing factors.

The function most commonly used by SRM designers takes the following form:

$$f_1 = T_{eAV} w^{-1} \tag{4}$$

where w is the electromagnetic torque ripple coefficient, determined as:

$$w = \frac{T_{eMAX} - T_{eMIN}}{T_{eAV}}, \tag{5}$$

were T_{eAV}, T_{eMIN}, and T_{eMAX} represent the average, minimum, and maximum values, respectively of electromagnetic torque.

The disadvantage of using an objective function in this form is its high susceptibility to single disturbances of the dependence of torque on its average value. Therefore, for the optimization process, solutions characterized by a very close dependence of the torque on the angle of rotation, in which single and temporal torque deviations from the average values are present, can be rejected. When using this criterion, solutions in which the maximum deviations of torque are characterized by the smallest amplitude, regardless of their number, are preferred. Objective function (4) represents the same value for both dependencies of torque on the angle of rotation, illustrated in Fig. 1.

In the case of the waveform shown in Fig. 1b, the electromagnetic torque ripple factor yields no information about its frequency.

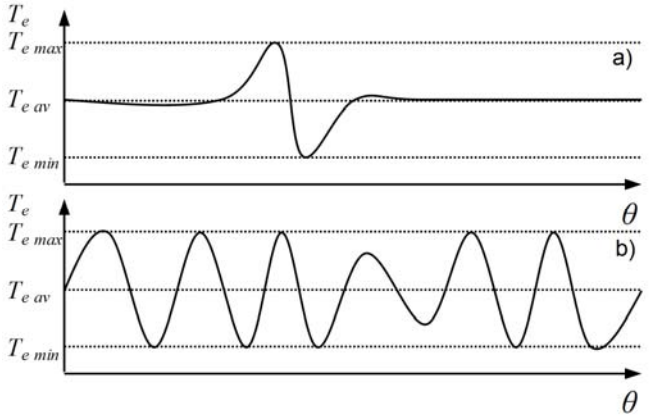

Figure 1. Characteristics of electromagnetic torque as a function of the angle of rotation with equal ripple coefficients: a) with a single disturbance, b) with disturbances in the whole range – overview.

In order to reduce the impact of single disturbances on the optimization result, the objective function was formulated as:

$$f_2 = T_{eAV} s^{-1} \tag{6}$$

where s is the standard deviation of electromagnetic torque in the range of phase power supply.

Within the optimization process, the dependence of torque on the angle of rotation was determined using a magnetic field distribution computation as part of the finite element method, assuming constant current density in windings. For all tested cases, the values of both demonstrated objective functions were computed, regardless of which one was the objective of this optimization.

The computations accounted for the fact that the core was made of a plate package processed according to a certain tolerance, dependent on the technology in use, usually ranging from 0.05 to 0.1 mm. Thus, in the drive design process, the optimization problem can be limited to a search for quasi-optimal solutions that meet the specified criteria, due to the correspondence of the tolerance to the core's selected production technology.

In the search for quasi-optimal solutions, good results can be obtained using stochastic methods, such as genetic algorithms [8, 20-24]. In general, these methods enable the discovery of near-optimal solutions in a relatively short period of time, regardless of the number of local extremes. However, their disadvantage is a lack of certainty about finding an accurate solution; moreover, the results are not repeatable.

For optimization computation, the genetic algorithm contained in the GAOT library of Matlab software was applied in the study. Previous studies using this library demonstrated that the obtained results are accurate and repeatable enough for the design of SRM machines. Differences in results obtained in different computation series were at the level of tolerances of production of the motor core.

The subject of optimization was a two-phase motor of 4/2 design; a cross section of its core is illustrated in Fig. 2. The core length of this motor is 120 mm. The motor supply voltage is 36 V. Windings were produced from copper turns with a diameter of 6.5 mm^2. A coil consisting of 15 turns was placed at each pole of the stator. Coils positioned on opposite poles were connected in series. The edge of the rotor was mapped by sixteen points that were connected with arcs, in which the applied genetic algorithm was able to change the position of fifteen turns in relation to the rotation centre of the rotor. The optimized measurands are indicated in Fig. 3; the ranges of acceptable changes to these measurands, adopted based on previous studies [17], are listed in Table 1.

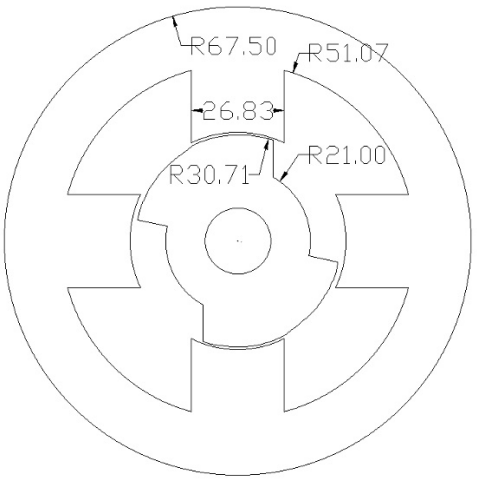

Figure 2. Cross-section of the optimized SRM core with marked dimensions (one of the obtained solutions)

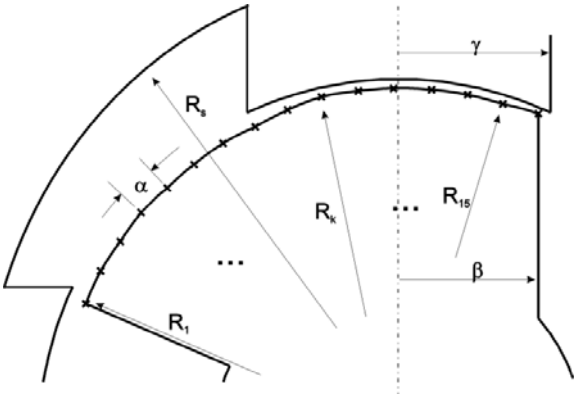

Figure 3. A fragment of the motor core with marked dimensions being optimized.

TABLE I. RANGE OF ACCEPTABLE CHANGES OF THE OPTIMIZED DIMENSIONS

Optimized parameters		Value	
Symbol	Description	min	max
γ	half of the stator tooth width (mm)	12	14.2
R_s	stator yoke thickness (mm)	16	17.5
β	rotor vertical edge relocation to the left from the axis (mm)	10	14
α	angular range between points in the rotor (deg)	5.3	6.5
R_1	radius at the beginning of sector 1 (mm)	29.45	29.85
R_2	radius at the boundary of sectors 1 and 2 (mm)	29.45	29.85
R_3	radius at the boundary of sectors 2 and 3 (mm)	29.45	29.85
R_4	radius at the boundary of sectors 3 and 4 (mm)	29.55	29.85
R_5	radius at the boundary of sectors 4 and 5 (mm)	29.55	29.85
R_6	radius at the boundary of sectors 5 and 6 (mm)	29.55	30.05
R_7	radius at the boundary of sectors 6 and 7 (mm)	29.55	30.05
R_8	radius at the boundary of sectors 7 and 8 (mm)	29.65	30.35
R_9	radius at the boundary of sectors 8 and 9 (mm)	29.95	30.45
R_{10}	radius at the boundary of sectors 9 and 10 (mm)	30.25	30.55
R_{11}	radius at the boundary of sectors 10 and 11 (mm)	30.35	30.65
R_{12}	radius at the boundary of sectors 11 and 12 (mm)	30.35	30.65
R_{13}	radius at the boundary of sectors 12 and 13 (mm)	30.35	30.65
R_{14}	radius at the boundary of sectors 13 and 14 (mm)	30.55	30.75
R_{15}	radius at the boundary of sectors 14 and 15 (mm)	30.55	30.75

Computations were performed in a distributed environment using HTCondor software. Each population generated by the software consisted of 42 individuals. The final criterion for computation was attainment of 100 populations. The objective function determination period for a single individual was approximately 3 minutes. For both studied objective functions (4) and (6), the computations were repeated three times. In the course of computation, the electromagnetic torque was determined by supplying the motor phase with a current of 90 A within a range of a rotor angle of rotation of π/2. It was assumed that the angle of rotation was zero when the rotor was characterized by minimum magnetic reluctance (rotor position as shown in Fig. 3). Results obtained in subsequent optimization series are listed in Table II.

TABLE II. RESULTS OF ROTOR TOOTH SHAPE OPTIMIZATION OF THE TWO PHASE SRM OBTAINED IN SUCCESSIVE SERIES DURING COMPUTATION

Type of objective function	Series no.	Value of objective function	*s*	T_{eAV}	*w*
$T_{eAV}s^{-1}$	***1***	***90.50***	**0.0495**	**4.4808**	**0.0385**
	2	*87.63*	0.0528	4.6268	0.0468
	3	*79.95*	0.0551	4.4029	0.0539
$T_{eAV}w^{-1}$	*1*	*59.11*	0.1260	4.7324	0.0800
	2	***66.31***	**0.1213**	**4.6492**	**0.0701**
	3	*50.46*	0.1622	4.7256	0.0936

Fig. 4 presents angular dependencies of the rotor radius length, obtained following optimization using both of the tested objective functions for which the highest values were obtained.

The dependencies of the electromagnetic torque on the rotor angle of rotation obtained for these designs, assuming the maximum value of phase current, are presented in Fig. 5. During operation, similar conditions occur only in the range of the lowest rotation speeds, when the drive operates in the current-limit mode. Rise and fall times of phase currents are then negligible compared to the duration of the phase supply cycle, whereas in the range of higher rotation speeds current waveforms in motor phases differ significantly from square waveforms.

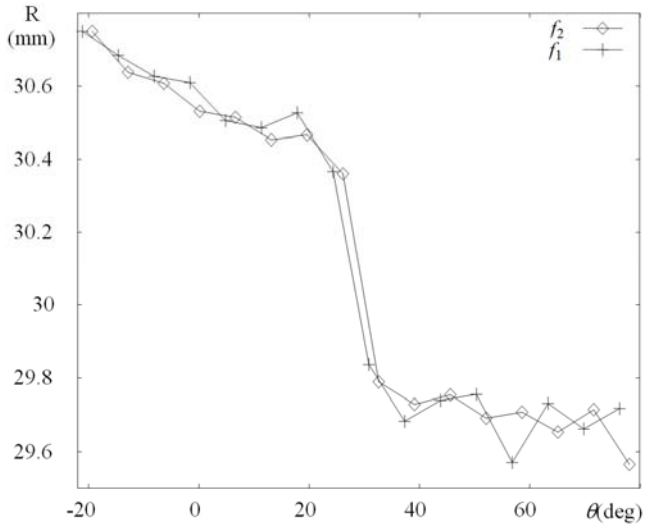

Figure 4. Radii of rotor edges as a function of the angle of rotation for the best results a) using the function (4), b) using the function (6)

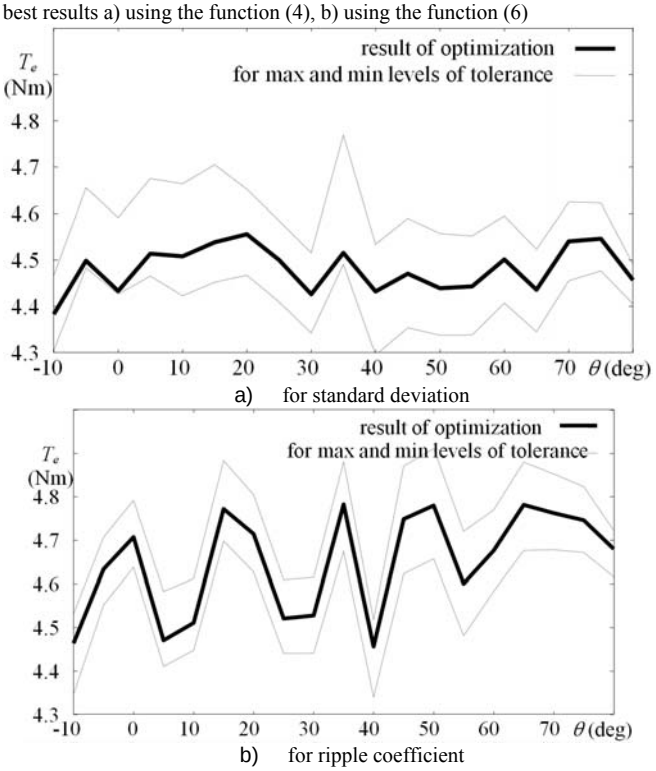

Figure 5. Overview of the electromagnetic torque on the rotor angle of rotation, expressed as a percentage of the maximum values of objective functions f_1 and f_2.

Fig. 6 presents electromagnetic torque characteristics for the best solution obtained using an objective function with standard deviation (6); Fig. 7 shows the electromagnetic flux

characteristic for the same case. In both figures, the phase current is a parameter taking values of 0, 4, 14, 36, 53, 65, 80, and 120 A.

As seen in Fig. 6, due to the non-linearity of the magnetic circuit, the nature of the electromagnetic torque characteristic varies depending on the phase current value. At lower values of phase current, it decreases with an increase in the angles, whereas at 140 A it increases. However, this static optimization does not consider normal operation conditions of the motor such as the phase current changes over time during a single rotation of the rotor.

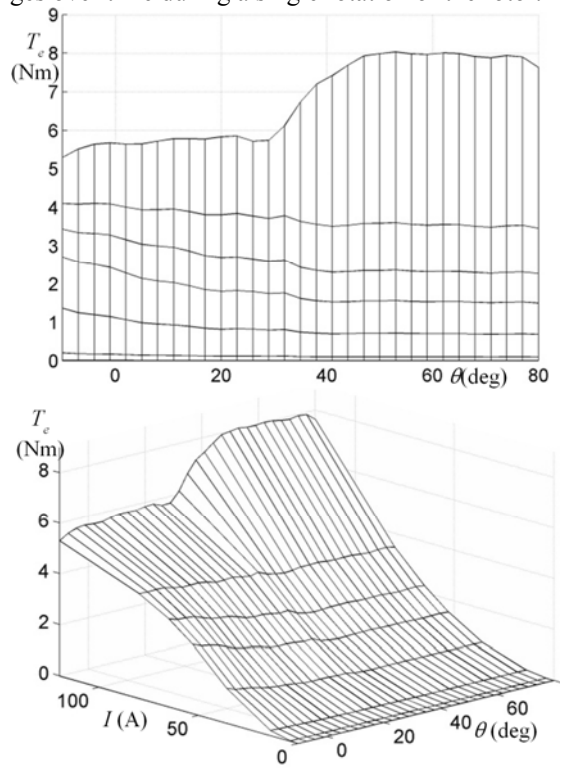

Figure 6. Overview of the electromagnetic torque on the rotor angle of rotation, with phase current as the parameter [0, 4, 14, 36, 53, 65, 80, 120A] for the best results using function (6)

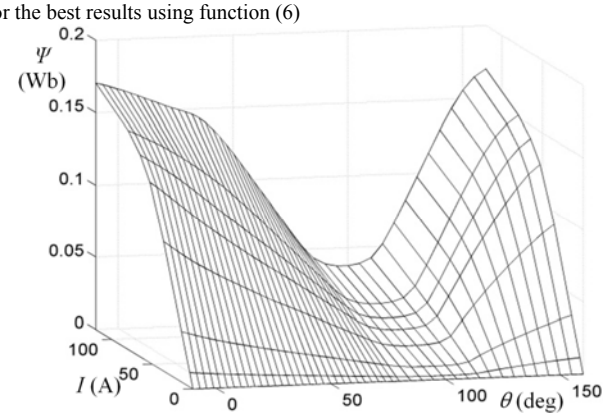

Figure 7. Electromagnetic flux over motor phase for the best results using function (6)

III. Calculations in the Simulation

For assessment of the quality of the obtained designs during operation of drives, a series of simulations were performed. An in-house simulation program, based on the mathematical model of a motor formulated as the Lagrange function, which uses array dependencies of the magnetic flux (Fig. 7) and the electromagnetic torque (Fig. 6) on the rotor angle of rotation and the phase current, was applied for this purpose. Mutual magnetic couplings between motor phases were not considered in the program.

Electromagnetic torque SRM T_e equals the delta of magnetic field coenergy W′ in the function of rotor angle θ

$$T_{\mathrm{e}} = \left.\frac{\partial \mathrm{W}'(\theta,\mathbf{i})}{\partial\theta}\right|_{\mathbf{i}=const} \tag{7}$$

whereas the coenergy of the magnetic field can be calculated as follows:

$$\mathrm{W}' = \int_0^{\mathrm{I_k}} \boldsymbol{\Psi}(\theta,\mathbf{i})\mathrm{d}\mathbf{i}^{\mathrm{T}} \tag{8}$$

were $\boldsymbol{\Psi}(\theta, \mathbf{i})$ is the vector of electromagnetic flux.

The Lagrange function L for a motor with m phases is as follows:

$$\mathcal{L} = \sum_{\mathrm{k=1}}^{\mathrm{m}} \int_0^{i_k} \Psi(\theta,\tilde{i})\mathrm{d}\tilde{i} + \frac{1}{2}J\dot{\theta}^2 . \tag{9}$$

The mathematical model equation:

$$\frac{\mathrm{d}}{\mathrm{dt}}\frac{\partial\mathcal{L}}{\partial\dot{q}} - \frac{\partial\mathcal{L}}{\partial q} = \frac{\partial(\delta\mathrm{A})}{\partial(\delta q)} \tag{10}$$

where

$$\delta\mathrm{A} = (\mathbf{u} - \mathbf{R}\cdot\mathbf{i})\boldsymbol{\delta}\mathbf{Q}^{\mathrm{T}} + (-T_l - D\dot{\theta})\partial\theta \tag{11}$$

represents virtual work done in the system.

According to (10) the equation for mechanical equilibrium takes the following form:

$$\frac{\mathrm{d}}{\mathrm{dt}}\frac{\partial\mathcal{L}}{\partial\dot{\theta}} - \frac{\partial\mathcal{L}}{\partial\theta} = -T_l - D\dot{\theta} . \tag{12}$$

For electric circuits

$$\frac{\mathrm{d}}{\mathrm{dt}}\frac{\partial\mathcal{L}}{\partial\dot{Q}_k} - \frac{\partial\mathcal{L}}{\partial Q_k} = u_k - R_k i_k \tag{13}$$

The final form of the equations of the mathematical model SRM, assuming no mutual magnetic coupling between the phases is represented by the expressions:

$$\mathrm{J}\frac{\mathrm{d}\omega}{\mathrm{d}t} = T_e - T_l - D\dot{\theta} \tag{14}$$

$$\frac{\mathrm{d}\Psi_k(\theta,i_k)}{\mathrm{d}t} = u_k - Ri_k, \qquad k = 1,2,...,N \tag{15}$$

where k – phase number, a N – number of all motor phases.

Because of the perpendicular position of the adjacent phase windings, mutual magnetic couplings in the tested SRM design occur only due to rotor asymmetry and the uneven saturation of the motor core, and their impact on the obtained results is much slighter than that of the non-linearity of the core magnetization characteristics (potentially introduced errors do not exceed 2%).

During the simulation, the motor was supplied from a common supply circuit composed of asymmetric H-bridges. The range width of the angle of rotation, where the phase was supplied, was assumed to be 90º. Computations were performed for power source voltages over a range of 10 to 36 V at every 1 V. Load torque was changed from 0.5 to 3.5 Nm at every 0.5 Nm. The switching angle of phase supply was also changed during the computations. The upper limit of the switching angle of the phase supply was determined based on the accepted range of changes of supply voltage and torque load; thus the maximum speed

value was obtained for a motor supply voltage of 36 V and a load of 0.5 Nm. The lower limit of changes in the angle was calculated at a voltage of 10 V and a load of 3.5 Nm. Thus the determined range of changes in the switching angle was equal to 19º. The computations were performed by changing the value of the switching angle by 1º. Consequently, the range of changes of power supply and load parameters covered 3,591 cases for each obtained version of the motor. In the course of the computations, values of two parameters for quality assessment of the obtained motor designs, i.e. standard deviation and torque ripple coefficient, were determined. Determination of values for a single case took approximately 4 minutes.

In 82.2% of cases, the standard deviation value of the electromagnetic torque waveform was lower for the solution obtained by using objective function (6). As well, the value of torque ripple coefficient was, in 63.8% cases, lower for designs obtained by applying objective function (6), in which standard deviations were considered.

Table 3 presents a quantitative overview of drive operation points expressed as a percentage of the obtained lower values of standard deviation and torque ripple coefficient, divided into ranges of power supply, mechanical power, rotation speed and an overall summary for all computed cases. Values presented in this table illustrate the percentage of cases in which designs obtained using function (6) were characterized by a smaller standard deviation or a lower torque ripple coefficient than designs determined using objective function (4).

TABLE III. OVERVIEW OF SOLUTIONS EXPRESSED AS A PERCENTAGE OF THE OBTAINED LOWER VALUES OF TORQUE RIPPLE (W) AND STANDARD DEVIATION (S) FOR DESIGNS DEVELOPED USING THE FUNCTION F2, IN RELATION TO THE OVERALL NUMBER OF TESTED CASES, DIVIDED INTO RANGES OF: SUPPLY VOLTAGE U, POWER P AND SPEED N.

	lower value of standard deviation	lower value of ripple coefficient
All cases	82.2%	63.8%
U < 24	81.4%	67.7%
24 <= U	83.0%	59.6%
P < 0.5	82.2%	66.3%
0.5 <= P < 1	81.7%	61.3%
1 <= P	83.5%	65.4%
n < 2000	79.4%	77.3%
2000 <= n < 4000	83.9%	60.3%
4000 <= n < 6000	77.0%	59.7%
6000 <= n	92.8%	57.9%

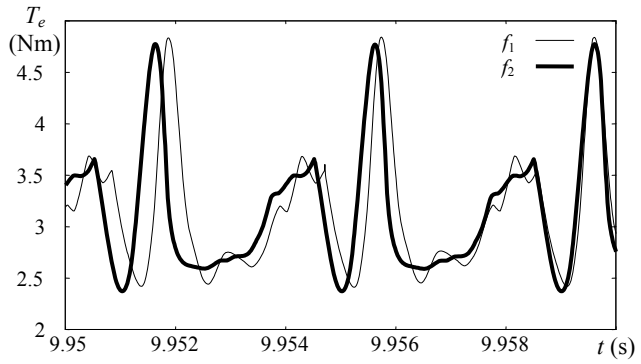

Figure 8. Electromagnetic torque waveforms during operation of both measured motor designs (load torque 3 Nm, supply voltage 36 V)

f_1 - design obtained by using torque ripple coefficient and a turn-off angle of -33°,

f_2 - design obtained by using torque standard deviation and a turn-off angle of -34°

Electromagnetic torque waveforms during operation of both motors at a load of 3 Nm and a supply voltage of 36 V are shown in Fig. 8.

IV. CONCLUSION

Designs derived from optimization for both objective functions used here are characterized by a relatively low comparable level of electromagnetic torque ripple. To define the objective function, standard deviations that improved linearization of torque dependence on the rotor angle of rotation were used. At most of the tested operating points, superior torque waveform parameters were obtained for the design optimized using function (6), considering the torque standard deviation. Designs obtained in three series of computations are characterized by repeatability sufficient for design purposes. Dimension differences obtained in successive series of optimization computations remain at an acceptable level for motor core plate processing. The objective function used here can also be successfully applied to SRMs with different designs.

In the two designs obtained during optimization, deterioration of electromagnetic torque waveform parameters could be observed during motor operation, compared to the dependencies obtained from optimization. This is due to phase current ripple, as magnetic circuit shapes were designed based on the assumption that their value was constant. This indicates that optimizing the magnetic circuit shapes based on the assumption of constant values of phase current is not very effective.

The obtained results indicate that the electromagnetic torque pulsation coefficient commonly used, i.e. (5), is not a sufficient quality ratio, as it is based on extreme values and does not take into account the shape of the rest of the electromagnetic torque waveform. Nor does it yield any information on the frequency spectrum of machine vibrations.

By additionally taking into account the value of standard deviation, it is possible to determine the quality of the electromagnetic torque waveform more precisely and to estimate its influence on the level and spectrum of machine vibrations

REFERENCES

[1] J. Furqani, M. Kawa, K. Kiyota, A. Chiba, "Current Waveform for Noise Reduction of a Switched Reluctance Motor Under Magnetically Saturated Condition," in IEEE Transactions on Industry Applications, vol. 54, no. 1, pp. 213-222, Jan.-Feb. 2018. doi:10.1109/TIA.2017.2756931

[2] Y. Mu, Y. Zhang, Z. Xie, M. Zhu, B. Zhao, "Control of torque ripple suppression and noise reduction of three-phase switched reluctance motor," Chinese Automation Congress (CAC), Jinan, 2017, pp. 2142-2147. doi:10.1109/CAC.2017.8243127

[3] H. Zeng, H. Chen, J. Shi, "Direct instantaneous torque control with wide operating range for switched reluctance motors," in IET Electric Power Applications, vol. 9, no. 9, pp. 578-585, 11 2015. doi:10.1049/iet-epa.2015.0087

[4] M. Mansouri Borujeni, A. Rashidi, S. M. Saghaeian Nejad, "Optimal four quadrant speed control of switched reluctance motor with torque ripple reduction based on EM-MOPSO," The 6th Power Electronics, Drive Systems & Technologies Conference (PEDSTC2015), Tehran, 2015, pp. 310-315. doi:10.1109/PEDSTC.2015.7093293

[5] R. Mikail, I. Husain, M. S. Islam, Y. Sozer, T. Sebastian, "Four-Quadrant Torque Ripple Minimization of Switched Reluctance Machine Through Current Profiling With Mitigation of Rotor Eccentricity Problem and Sensor Errors," in IEEE Transactions on

Industry Applications, vol. 51, no. 3, pp. 2097-2104, May-June 2015. doi:10.1109/TIA.2014.2365715

[6] H. Zeng, H. Chen, J. Shi, "Direct instantaneous torque control with wide operating range for switched reluctance motors," in IET Electric Power Applications, vol. 9, no. 9, pp. 578-585, 11 2015. doi:10.1049/iet-epa.2015.0087

[7] Y. Li, D. C. Aliprantis, "Optimum stator tooth shapes for torque ripple reduction in switched reluctance motors," International Electric Machines & Drives Conference, Chicago, IL, 2013, pp. 1037-1044. doi:10.1109/IEMDC.2013.6556224

[8] Y. Zhang, B. Xia, D. Xie, C. S. Koh, "Optimum design of switched reluctance motor to minimize torque ripple using ordinary Kriging model and genetic algorithm," International Conference on Electrical Machines and Systems, Beijing, 2011, pp. 1-4. doi:10.1109/ICEMS.2011.6073924

[9] J. Ye, B. Bilgin, A. Emadi, "An Offline Torque Sharing Function for Torque Ripple Reduction in Switched Reluctance Motor Drives," in IEEE Transactions on Energy Conversion, vol. 30, no. 2, pp. 726-735, June 2015. doi:10.1109/TEC.2014.2383991

[10] J. Zhu, K. W. E. Cheng, X. Xue, Y. Zou, "Design of a New Enhanced Torque In-Wheel Switched Reluctance Motor With Divided Teeth for Electric Vehicles," in IEEE Transactions on Magnetics, vol. 53, no. 11, pp. 1-4, Nov. 2017. doi:10.1109/TMAG.2017.2703849

[11] J. W. Jiang, B. Bilgin, A. Emadi, "Three-Phase 24/16 Switched Reluctance Machine for a Hybrid Electric Powertrain," in IEEE Transactions on Transportation Electrification, vol. 3, no. 1, pp. 76-85, March 2017. doi:10.1109/TTE.2017.2664778

[12] S. R. Mousavi-Aghdam, M. R. Feyzi, N. Bianchi, M. Morandin, "Design and Analysis of a Novel High-Torque Stator-Segmented SRM," in IEEE Transactions on Industrial Electronics, vol. 63, no. 3, pp. 1458-1466, March 2016. doi:10.1109/TIE.2015.2494531

[13] X. Deng, B. Mecrow, H. Wu, R. Martin, "Design and Development of Low Torque Ripple Variable-Speed Drive System With Six-Phase Switched Reluctance Motors," in IEEE Transactions on Energy Conversion, vol. 33, no. 1, pp. 420-429, March 2018. doi:10.1109/TEC.2017.2753286

[14] E. K. Beser, S. Camur, B. Arifoglu, E. Beser, "Design and Analysis of an Axially Laminated Reluctance Motor for Variable-Speed Applications," Advances in Electrical and Computer Engineering, vol.13, no.1, pp.75-80, 2013. doi:10.4316/AECE.2013.01013

[15] S. Cai, J. Shen, H. Hao, M. Jin, "Design methods of transversally laminated synchronous reluctance machines," in CES Transactions on Electrical Machines and Systems, vol. 1, no. 2, pp. 164-173, 2017. doi:10.23919/TEMS.2017.7961338

[16] H. A. Moghaddam, A. Vahedi, S. H. Ebrahimi, "Design Optimization of Transversely Laminated Synchronous Reluctance Machine for Flywheel Energy Storage System Using Response Surface Methodology," in IEEE Transactions on Industrial Electronics, vol. 64, no. 12, pp. 9748-9757, Dec. 2017. doi:10.1109/TIE.2017.2716877

[17] M. Lukaniszyn, K. Tomczewski, A. Witkowski, K. Wrobel, M. Jagiela. "Rotor Shape Optimization of a Switched Reluctance Motor." Monograph Intelligent Computer Techniques in Applied Electromagnetics, Applications of Computer Methods, Springer 2008; Berlin, vol. 119, pp. 217 – 221. doi:10.1007/978-3-540-78490-6

[18] P. Bogusz, M. Korkosz, A. Powrozek, J. Prokop, "A two-phase switched reluctance motor with reduced stator pole-arc," International Conference on Electrical Drives and Power Electronics (EDPE), Tatranska Lomnica, 2015, pp. 312-318. doi:10.1109/EDPE.2015.7325312

[19] Kano, T. Kosaka, N. Matsui, "Optimum Design Approach for a Two-Phase Switched Reluctance Compressor Drive," in IEEE Transactions on Industry Applications, vol. 46, no. 3, pp. 955-964, May-june 2010. doi:10.1109/TIA.2010.2045212

[20] R. T. Naayagi, V. Kamaraj, "A Comparative Study of Shape Optimization of SRM using Genetic Algorithm and Simulated Annealing," Annual IEEE India Conference - Indicon, 2005, pp. 596-599. doi:10.1109/INDCON.2005.1590241

[21] J. Zhang, H. Wang, L. Chen, C. Tan, Y. Wang, "Multi-Objective Optimal Design of Bearingless Switched Reluctance Motor Based on Multi-Objective Genetic Particle Swarm Optimizer," in IEEE Transactions on Magnetics, vol. 54, no. 1, pp. 1-13, Jan. 2018. doi:10.1109/TMAG.2017.2751546

[22] C. Lopez, T. Michalski, A. Espinosa, L. Romeral, "Rotor of synchronous reluctance motor optimization by means reluctance network and genetic algorithm," XXII International Conference on Electrical Machines (ICEM), Lausanne, 2016, pp. 2052-2058. doi:10.1109/ICELMACH.2016.7732805

[23] M. H. Mohammadi, T. Rahman, R. Silva, M. Li, D. A. Lowther, "A Computationally Efficient Algorithm for Rotor Design Optimization of Synchronous Reluctance Machines," in IEEE Transactions on Magnetics, vol. 52, no. 3, pp. 1-4, March 2016. doi:10.1109/TMAG.2015.2491306

[24] T. Raminosoa, B. Blunier, D. Fodorean, A. Miraoui, "Design and Optimization of a Switched Reluctance Motor Driving a Compressor for a PEM Fuel-Cell System for Automotive Applications," in IEEE Transactions on Industrial Electronics, vol. 57, no. 9, pp. 2988-2997, Sept. 2010. doi:10.1109/TIE.2010.2041133